

# An Efficient Segmentation Method for Juxtapleural Parenchyma with Modified Fractal Geometry-Based Pulmonary Boundary Detection



S.Vaishali, G.V.Subba Rao, K.Kishan Rao

**Abstract:** Lung cancer seems to be the world has ever known the most leading cause of death from cancer. Early diagnosis of lung cancer will help patients significantly. The exactness of tumour form, location, and volume detection wants to play an important role to play in effective tumour treatment. Artefacts can severely deteriorate the performance or even clinically obsolete of computed tomographic (CT) images. An automatic approach to incorporate the adaptive threshold iteration technique with the segmentation of images of the lungs. The implementation involves an enhanced convex hull repair to undertake a precise lung parenchyma segmentation. The results of the analysis say with certainty that the current approach can precisely segment juxtapleural parenchymal images and that the algorithm has been put into practice and evaluated in Matlab on Windows. The investigation results indicate that the modified convex hull calculation uses only a very small number of points. The study has also shown that the algorithm proposed improves the complexity of time compared to several other algorithms.

**Keywords:** lung cancer; CT-image; lung parenchymal segmentation; juxtapleural nodules

## I. INTRODUCTION

Cancer is the productivity of cells that are abnormally and indiscriminate. The adjacent tissue can be damaged far from its origin. If cancer can indeed be identified and treated early, the rate of deaths can reduce, the chance of growth will be higher. Early diagnosis of lung cancer will contribute to the patient's recovery. CT scan (Computed Tomography) is a tool for detecting lung cancer. The CT scan image requires different results between normal and abnormal lungs, as well as the stage of lung cancer. In this way, the inspection process normally requires equipment that is very complex, costly and requires process experts. Yet professionals can make errors when trying to separate normal from abnormal lungs. Essentially manual segmentation of CT images for measuring lung tumour volume, which depends on the operator and is time-consuming.

**Revised Manuscript Received on December 30, 2019.**

\* Correspondence Author

**S.Vaishali\***, Research Scholar, Department of ECE, KLEF, Vijayawada, Andhra Pradesh, India.

**Dr.G.V.Subba Rao** Professor, Department of ECE, KLEF, Vijayawada, Andhra Pradesh, India.

**Dr.K.Kishan Rao**, Professor, Department of ECE, Sreenidhi Institute of Science and Technology, Hyderabad, (Telangana), India.

© The Authors. Published by Blue Eyes Intelligence Engineering and Sciences Publication (BEIESP). This is an [open access](https://creativecommons.org/licenses/by-nc-nd/4.0/) article under the CC-BY-NC-ND license <http://creativecommons.org/licenses/by-nc-nd/4.0/>

Segmentation is a process through which the region of interests of a digital image is divided into different segments using properties like intensity, texture, etc. that can be analyzed much easier. Lung segmentation errors would produce false information, so precise segmentation is required [1]. Therefore, morphological operations with k-mean clustering are used in earlier works for stronger segmentation methods such as thresholding. Even though the CT scan offers stronger pulmonary imaging, it is hard to automatically identify the tumour. Computer-aided detection (CAD) is therefore conducted for the segmentation of the tumour nodule. Research teams suggested different techniques for segmentation of the tumour nodule. Clinicians often perform manual segmentation [2] which depends on the operator and is usually faulty. Manual separation of tumour volumes is, difficult and past research has also shown that semi-automatic computer generated segmentations are replicable rather than manual demarcations, particularly with regard to radiomics analysis [4]. Semi-automatic techniques to lung cancer semi-segmentation provide one-click ensemble techniques [5] and a watershed marker controlled process [6]. Furthermore, these techniques, when introduced to the segmentation of lung nodule [7], produce different results [8]. The proposed algorithm is based on the Niblack thresholding and improved convex hull algorithm [11]. Interactive methodology [9, 10] that confirm its segments to user input is affected by an interrater variability. After the juxtapleural nodule segmentation has been finished, the proposed algorithm uses a fractal geometry method to detect the concave boundary of the studied concave area and, subsequently, uses an enhanced convex-hull algorithm, in order to produce a precise segmentation of the lung parenchyma. The main contributions and organization of this paper are summarized as follows: In section 2 we describe background details of lung nodule detection. Section3 discusses the proposed work. Section 4 deliberates results and discussions. Finally, in section 5, we concluded the paper.

## II. BACKGROUND WORKS

A lonely (parenchymal, non-pleural) lung nodule in the lungs is a tiny, round or egg-formed lesion. The juxtapleural lung nodule is a small, worm-shaped lesion associated with pleura as shown in Figure 1. If we note that the image intensity varies in several slices of the CT stack of a patient, a fixed threshold is not appropriate for all slices.



# An Efficient Segmentation Method for Juxtapleural Parenchyma with Modified Fractal Geometry-Based Pulmonary Boundary Detection

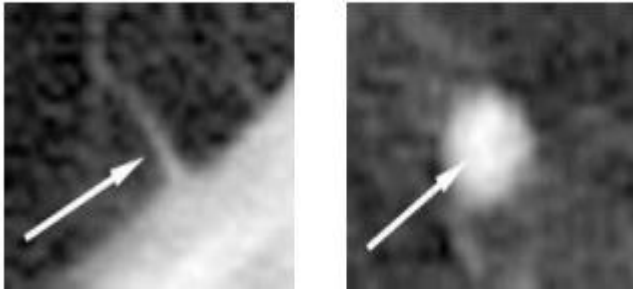


**Figure .1: Nodule examples: juxtapleural nodule (left), parenchymal nodule (right)**

We suggest an appropriate threshold for the automatic segmentation of the lungs in CT images in this paper. The suggested technique determines the right limit for each CT slice and automatically divides the lung. This algorithm also uses the mean and variation of pixel intensities to completely extract big airways. Such airways differ in place, size, amount and are hard to identify.

In pulmonary CT images the air appears at the mean intensity of approximately -1000 Hounsfield Units (HU), the area of the pulmonary area is within the range between -1000 and -400 HU and the chest wall, with the blood and bone density above-400 HU[12].

1. The smallest FN frequency (amount of nodules lost).
2. Robustness (sound, image resolution, etc.).
3. Output relevance (small amount of FPs per slice).

### III. PROPOSED WORK

This section offers an algorithm to accurately segment pulmonary parenchyma with juxtapleural traction nodules. This algorithm involves the original segmentation of CT images with automatic limit iteration, bronchial tissue extraction, and lung boundary detection.

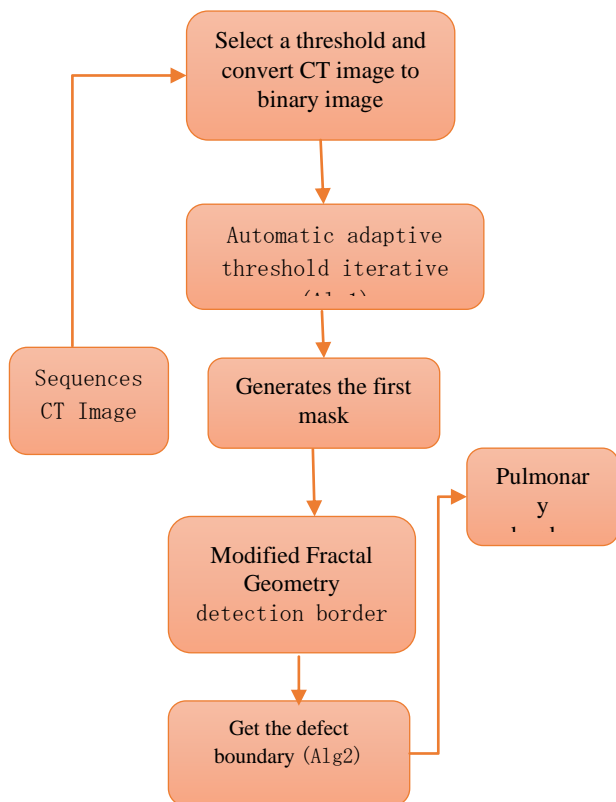


**Figure.2: Flow diagram of the lung parenchyma segmentation algorithm.**

Figure 2 shows the pulmonary parenchyma algorithm flow. To avoid missing significant data on the segmentation of the pulmonary parenchyma, such noise was allowed. Open and near activities were used during this section to smooth and complete the border and inside of the pulmonary parenchyma.

### Automated Adaptive Threshold Iterative Segmentation of Sequential CT Image (Algorithm 1):

An appropriate global limit is hard to choose when to achieve the optimal original contour due to variations in the grey concentrations of pulmonary nodules. Considering the elevated correlation among neighbouring sequential CT image slices, the automated threshold iteration technique was adopted to build the original contours of a linear CT image pulmonary parenchyma, the algorithm can be seen in the Algorithm 1. In Figure 3, the first row indicates the initial of a linear CT image with (a–d) a series of images and the second line outcomes of the automatic threshold iterative pulmonary parenchyma segmentation.

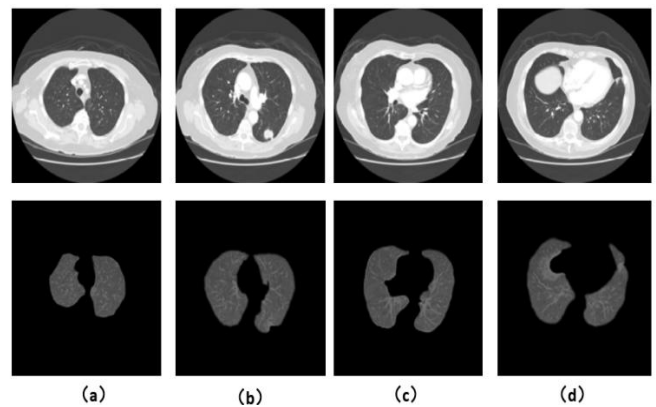


**Figure. 3: Results of the automated adaptive threshold iterative segmentation of lung parenchyma**

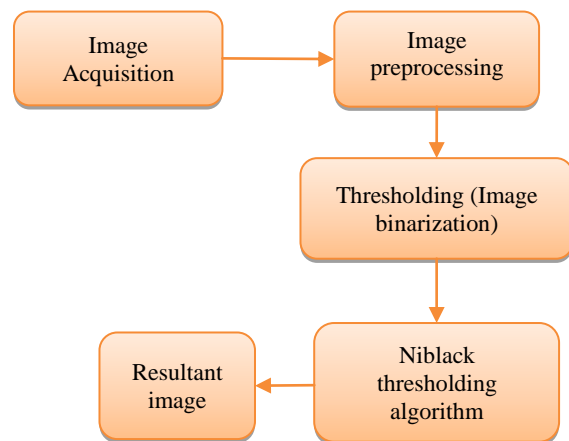


**Figure.4: flow process of thresholding**

Upon completion of the original segmentation, the automated threshold iteration technique could obtain a pulmonary parenchyma image. At the same time, the respective global optimum limit  $T$  could be achieved. Image  $I(x, y)$  can be transformed by Formula (1) into a binary image  $I_{bin}(x, y)$

$$I_{bin}(x, y) = \begin{cases} 1, & (x, y) \geq T \\ 0, & I(x, y) < T \end{cases} \quad (1)$$

A quick way to execute the Niblack binarization algorithm is outlined. It employs not just the integral image for calculating the local mean values, as well as the integral image of the second order for calculating the local variance. Having followed the proposed strategy, the time of segmentation has been drastically reduced delivering the possibility of its use in practice. The idea of the Niblack method is to calculate the binarization threshold  $T(x, y)$  by local mean  $m(x, y)$  and standard deviation  $s(x, y)$  of the neighbouring pixel intensity values:

$$T(x, y) = m(x, y) + k \cdot s(x, y) \quad (2)$$

The local average value in (2) can be computed efficiently using an integral image from the original image is computed. The local average value in (2) could be computed efficiently with integral image depiction. Complete image from the initial  $f(x, y)$  is computed as follows.

$$I(x_0, y_0) = \sum_{x=1}^{x_0} \sum_{y=1}^{y_0} f(x, y) \quad (3)$$

With the integral image, the average local value increased by the number of region pixels in the rectangle region can only be computed using additional tree activities:

$$\begin{aligned} m(x_0, y_0) \cdot N &= I(x_0 + \Delta x, y_0 + \Delta y) \\ &+ I(x_0 - \Delta x - 1, y_0 - \Delta y - 1) \\ &- I(x_0 - \Delta x - 1, y_0 + \Delta y) \\ &- I(x_0 + \Delta x, y_0 - \Delta y - 1) \end{aligned} \quad (4)$$

Where  $m(x_0, y_0)$  local mean value inside rectangle area with centre coordinates  $(x_0, y_0)$ .

$(x_0 - \Delta x, y_0 - \Delta y)$  and  $(x_0 + \Delta x, y_0 + \Delta y)$  are upper left and the lower right corners coordinates.

The generalization of integral image representation is  $k$ -order integral image:

$$I_k(x_0, y_0) = \sum_{x=1}^{x_0} \sum_{y=1}^{y_0} [f(x, y)]^k \quad (5)$$

The depiction (4) could be used accurately to calculate the  $k$ -order local statistical data in the same way as the local average value (4). The initial time loss during Niblack binarization is linked to the computation of a local standard image-pixel intensity deviation. A second-order integral image depiction would be used to speed these calculations:

$$I_2(x_0, y_0) = \sum_{x=1}^{x_0} \sum_{y=1}^{y_0} [f(x, y)]^2 \quad (6)$$

Taking into consideration the well-known analysis of the statistics in which the variance is calculated as the distinction between the average square value and the average value, it could be computed as given using the second class integral image depiction (6):

$$\begin{aligned} s^2(x_0, y_0) \cdot (N - 1) &= I_2(x_0 + \Delta x, y_0 + \Delta y) \\ &+ I_2(x_0 - \Delta x - 1, y_0 - \Delta y - 1) \\ &- I_2(x_0 - \Delta x - 1, y_0 + \Delta y) \\ &- I_2(x_0 + \Delta x, y_0 - \Delta y - 1) \\ &- \frac{1}{N} \cdot [m(x_0, y_0) \cdot N]^2 \end{aligned} \quad (7)$$

Table 1 provides the simplicity of calculating the local normal value for the area of occurrence of adjudgment using the suggested integral depiction it can sometimes be evident that the integrated image representation of the second-order significantly reduces the complexity and autonomy of the calculations in the local window area  $N$ .

**Table 1. The computational complexity of calculation of local standard deviation directly and using the proposed integral representation**

Operation	Number of operations	
	By direct calculation	Using integral representation $I_2$
Addition/subtraction	$1+(2N-1)N_1N_2$	$1+3N_1N_2-N_1-N_2$
Multiplication/squaring	$1+(N+1)N_1N_2$	$1+4N_1N_2$
Division	1	1
Squaring rooting	$N_1N_2$	$N_1N_2$

The Niblack Binarization Threshold for one pixel is calculated by immediate computation of the local average and the normal deviation values in the local  $N$  window, by roughly adding activities, dividing and squaring and by one column rooting. The use of integral depictions (3) and (6) allows for autonomy from the local window region and a decrease of about 12 additional mathematical operations, four multiplications, two squared and one square rooting per local calculation of limit value.

The primary algorithmic flow for calculating the binarization limit value is as below:

- Locate out the mean value of the image (global average—this is only calculated once per image).
- Evaluate image default value (global default deviation only calculated once per image).
- Set the volume of the local area by pixel area (usually referred to as window width).
- Pick a suitable local window size area for each pixel from the image bit by bit.
- Calculate the median (local mean) of that area and the normal area variation (local normal deviation) for each local area.
- Fixing the weight ' $k$ ' value for each local window with (5). It uses local mean, normal deviation, global mean and standard deviation.
- Apply (2) to evaluate the local mean limit value and the default for each local area.
- Relate a limit value to the single pixel that selects the local window.
- Change the increment window by one pixel and go to stage 4 to calculate the next pixel limit.
- Fine-tuned when the limit is calculated and implemented to the entire image region. (The outcome after this stage is an image that only has a binary image on two layers).



This implies, of course, that we need a basic reality for contrast. The Jaccard coefficient  $J$  estimates the proportion of the two sets of junction ( $A$  and  $B$ ) split by the region of their location,

$$J = \frac{|A \cap B|}{|A \cup B|}$$

The ratio of the Jaccard varies between 0 and 1, with 1 that matches perfect classifications. The non-uniform area measurement indicates the intrinsic value of the segmented area. Assume that  $f(x, y)$  is grayscale and RNU is described as a region non-uniformity.

$$RNU = \frac{|FG| \times Var(FG)}{|FG + BG| \times Var(f)}$$

Where  $FG$  is the foreground image pixel, and  $BG$  is the background image pixel, So the variance of the full image denoted by  $Var(f)$  and  $Var(FG)$  reflects the foreground image area  $f(x, y)$ ,  $|.$ the cardinality of that object. The strong segmented image is near to 0 with an  $RNU$  significance.

**Time complexity:** The algorithm was also evaluated for time complexity. We compared the processing time of different CT images and the average time that was consumed for segmenting the sequence of CT images.

**For Image 1:**

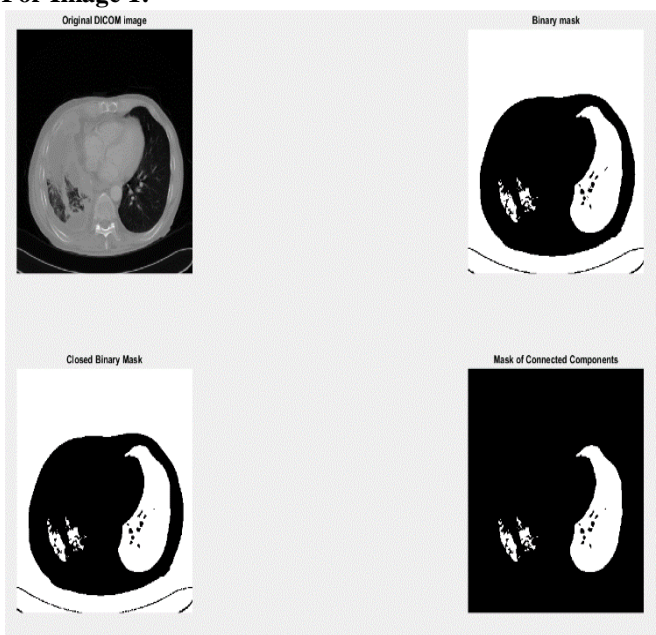


Figure 6: morphological operations

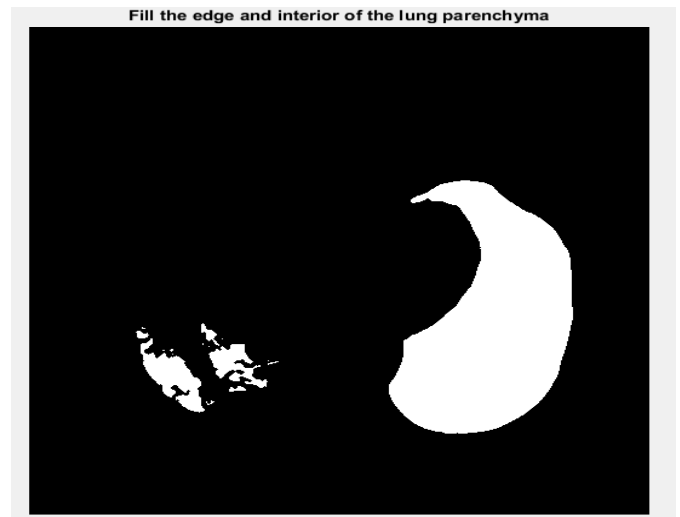


Figure 7: Edge and interior of lung parenchyma

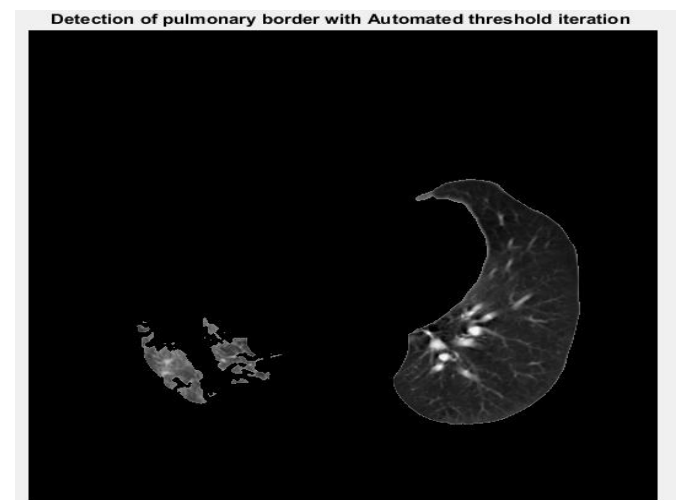


Figure 8: After automated thresholding

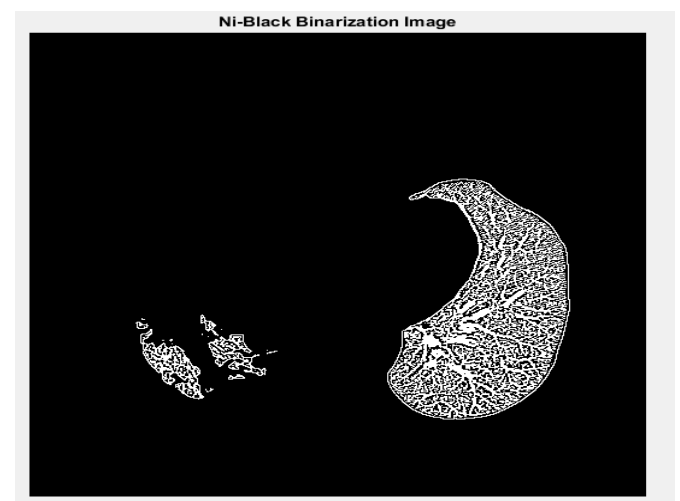


Figure 9: After Niblack binarization

# An Efficient Segmentation Method for Juxtapleural Parenchyma with Modified Fractal Geometry-Based Pulmonary Boundary Detection

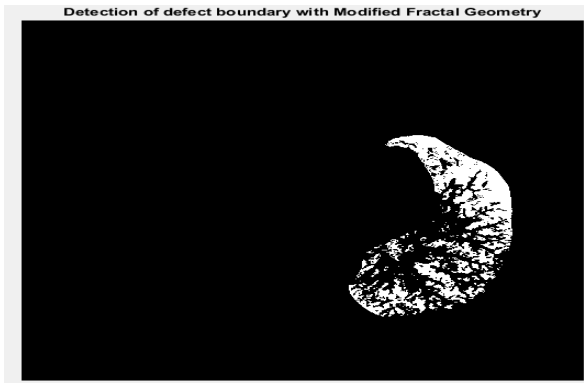


Figure 10: After boundary detection using Fractal geometry

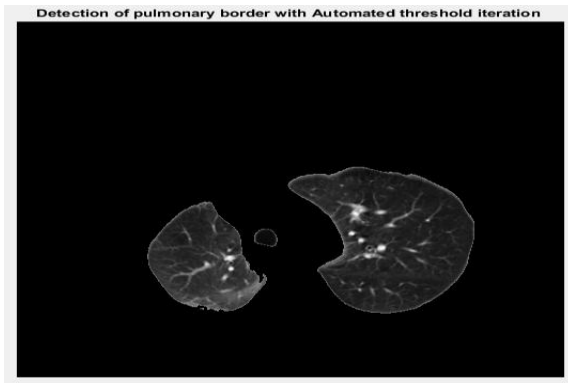


Figure 14: After automated thresholding

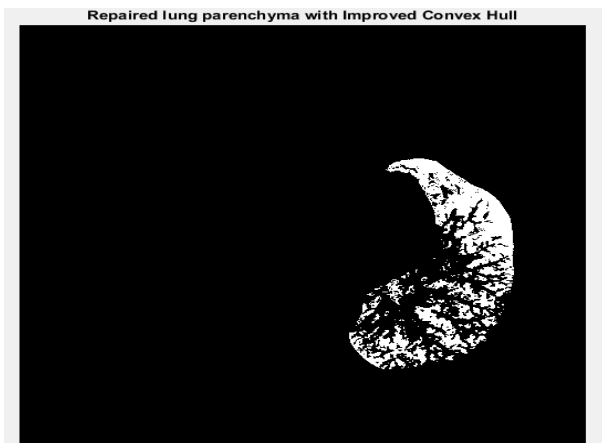


Figure 11: Repaired lung parenchyma with improved Convex hull

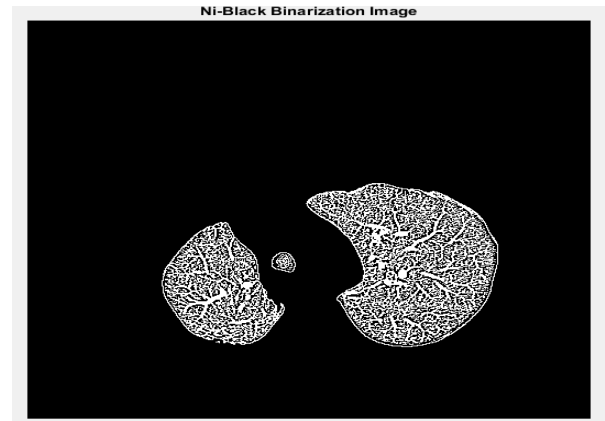


Figure 15: After Niblack binarization

For Image 2:

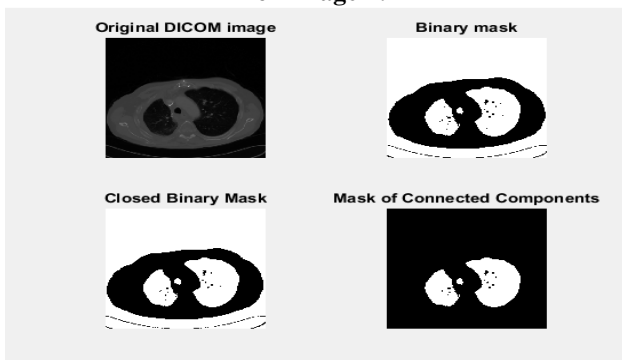


Figure 12: morphological operations

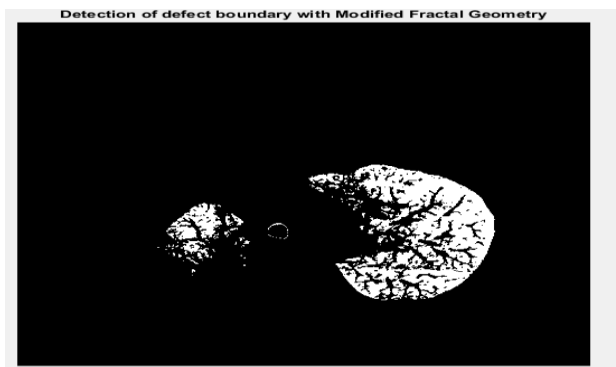


Figure 16: After boundary detection using Fractal geometry

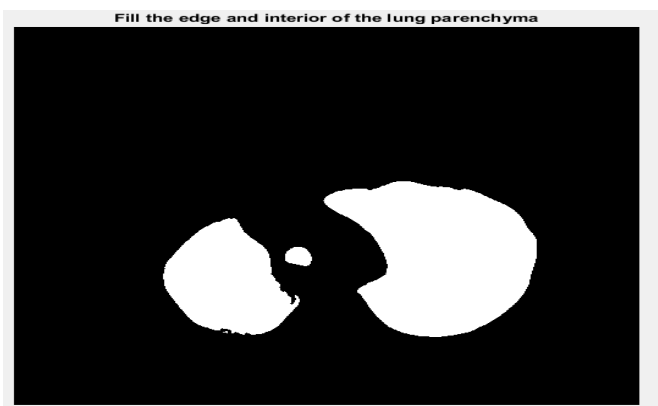


Figure 13: Edge and interior of lung parenchyma

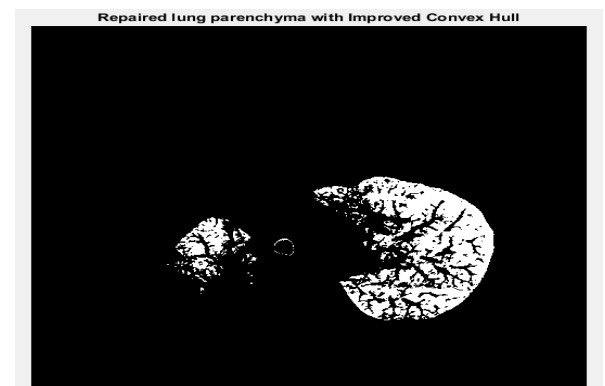
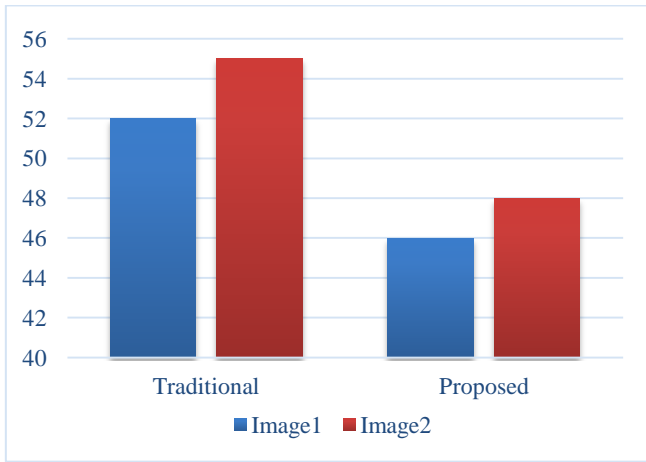


Figure 17: Repaired lung parenchyma with improved Convex hull



**Figure 18: Processing time of Images**

The algorithm was indeed assessed for the complexity of time. As shown in Figure.18, the technique suggested was processed in the shortest time was 46sec for image1 and 48sec for image2. The traditional algorithm was processed for the more time was 52sec for image1 and 55sec for image2.

Table.2 shows clearly the Jaccard coefficient of conventional technique and proposed technique for all the CT images considered in this Matlab R2017a software for algorithm implementation. Our proposed technique gives a very high score of 99.5% to the under segmented lung nodule results on Image1, whereas the traditional technique is 99.2%.

**Table 2: Jaccard coefficient of Traditional Technique and proposed Technique**

CT images	Traditional Technique (J)	Proposed Technique (J)
Image1	0.992	0.995
Image2	0.866	0.898
Image3	0.913	0.945
Image4	0.894	0.915
Image5	0.832	0.923

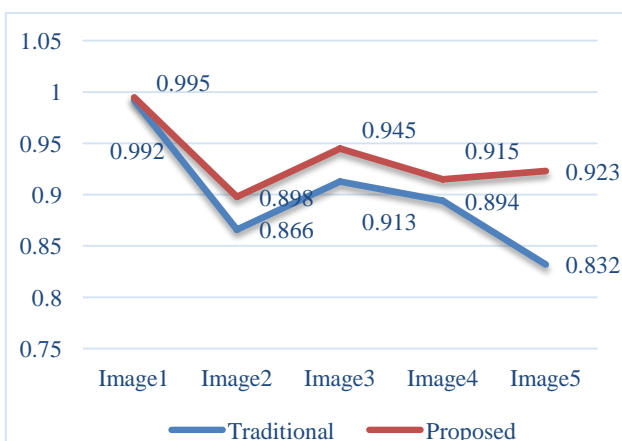


**Figure 19: Comparison of Medical images using Jaccard coefficient**

It is clear from the Fig.19 the Jaccard coefficient for proposed technique is better as compared to traditional technique due to our adaptive thresholding technique that removes automatically background by using local mean and standard deviation which makes segmentation easier.

**V. CONCLUSION**

The optimum limit for every patient CT collection relies on the following fundamental variables: tissue and fluid volume, tissue density units, image procurement methods and pulmonary parenchyma image contrast. For each image in the chosen sequence, the optimum adaptive limit is also chosen. We introduced an automatic nodule detection technique. In this paper, a dedicated segmenting method for sequential CT images is suggested for the identification juxtapleural nodules based on the rapid Niblack binarization algorithm and the enhanced convex hull matrix. The use of the second order integral image offers quick variance calculation (and normal deviation). Local data of greater order can be further calculated with greater order integral imaging. The suggested technique was used to introduce quick Niblack binarization algorithms for microscopic lung nodules image segmentation. The assessment findings were contrasted by qualified radiologists with the outcomes of manual segmentation. To conclude, the results of our current investigation give preference to time complexity and Jaccard similarity coefficients over proposed and traditional techniques.

**ACKNOWLEDGEMENT**

Authors would like to express sincere gratitude to management and principal of KLEF, Vijayawada, Andhra Pradesh, India, for their support and encouragement to carry out the research work

**REFERENCES**

1. A. Mansoor et al., "Segmentation and Image Analysis of Abnormal Lungs at CT: Current Approaches, Challenges, and Future Trends," Radiographic, vol. 35 no. 4 pp. 1056-1076, 2015.
2. J. Wang et al., "Prediction of Malignant and Benign of Lung Tumor using a Quantitative Radiomic Method," Proceedings of International Conference of the IEEE Engineering in Medicine and Biology Society(EMBC), pp. 1272-1275, 2016.
3. E. R. Velazquez, C. Parmar, M. Jermoumi, R. H. Mak, A. Van Baardwijk, F. M. Fennessy, et al., "Volumetric CT-based segmentation of NSCLC using 3D-Slicer," Scientific reports, vol. 3, pp. 3529, 2013.
4. C. Parmar, E. R. Velazquez, R. Leijenaar, M. Jermoumi, S. Carvalho, R.H. Mak, et al., "Robust radiomics feature quantification using semiautomatic volumetric segmentation," PloS one, vol. 9, pp. e102107, 2014.
5. Y. Gu, V. Kumar, L. O. Hall, D. B. Goldgof, C.-Y. Li, R. Korn, et al., "Automated delineation of lung tumours from CT images using a single click ensemble segmentation approach," Pattern Recognition, vol. 46, pp. 692-702, 2013.
6. Y. Tan, L. H. Schwartz, and B. Zhao, "Segmentation of lung lesions on CT scans using watershed, active contours, and Markov random field," Medical physics, pp.043502, vol. 40, 2013.
7. J. Kalpathy-Cramer, B. Zhao, D. Goldgof, Y. Gu, X. Wang, H. Yang, et al., "A comparison of lung nodule segmentation algorithms: methods and results from a multi-institutional study," Journal of digital imaging, vol. 29, pp. 476-487, 2016.
8. Y. Balagurunathan, A. Beers, J. Kalpathy-Cramer, M. McNitt- Gray, L. Hadjiiski, B. Zhao, et al., "Semi-automated pulmonary nodule interval segmentation using the NLST data," Medical Physics, vol. 45, pp. 1093-1107, 2018.
9. O. Grove, A. E. Berglund, M. B. Schabath, H. J. Aerts, A. Dekker, H.Wang, et al., "Quantitative computed tomographic descriptors associate tumour shape complexity and intratumor heterogeneity with prognosis in lung adenocarcinoma," PloS one, vol. 10, p. e0118261, 2015.
10. J. Egger, T. Kapur, A. Fedorov, S. Pieper, J. V. Miller, H.Veeraraghavan, et al., "GBM volumetry using the 3D Slicer medical image computing platform," Scientific Reports, vol. 3, 2013.



## An Efficient Segmentation Method for Juxtapleural Parenchyma with Modified Fractal Geometry-Based Pulmonary Boundary Detection

11. H. Veeraraghavan, B. Z. Dashevsky, N. Onishi, M. Sadinski, E. Morris, J. O. Deasia, et al., "Appearance Constrained Semi-Automatic Segmentation from DCE-MRI is Reproducible and Feasible for Breast Cancer Radiomics: A Feasibility Study," Scientific Reports, vol. 8, p.4838, 2018.
12. M. S. Brown, M. F. Mcnittgray, N. J. Mankovich, J. G. Goldin, J. Hiller, L. S. Wilson, and D. R. Aberle, "Method for segmenting chest CT image data using an anatomical model - preliminary results," IEEE Trans Medical Imaging, vol. 16, 828-839, 1997.